JACS
JOURNAL OF THE AMERICAN CHEMICAL SOCIETY

Article

pubs.acs.org/JACS

Bacteriophage Tailspikes and Bacterial O-Antigens as a Model System to Study Weak-Affinity Protein–Polysaccharide Interactions

Yu Kang,[†,#,⊗] Ulrich Gohlke,[‡,⊗] Olof Engström,[§,⊗] Christoffer Hamark,[§] Tom Scheidt,[∥,▽] Sonja Kunstmann,[∥] Udo Heinemann,[‡,⊥] Göran Widmalm,[§] Mark Santer,*[,†] and Stefanie Barbirz*[,∥]

[†]Max Planck Institute of Colloids and Interfaces, Am Mühlenberg 1, 14476 Potsdam, Germany

[‡]Max-Delbrück-Centrum für Molekulare Medizin in der Helmholtz-Gemeinschaft, Robert-Rössle-Str. 10, 13125 Berlin, Germany

[§]Department of Organic Chemistry, Arrhenius Laboratory, Stockholm University, S-106 91 Stockholm, Sweden

[∥]Physikalische Biochemie, Universität Potsdam, Karl-Liebknecht-Str. 24-25, 14476 Potsdam, Germany

[⊥]Institut für Chemie und Biochemie, Freie Universität, Takustr. 6, 14195 Berlin, Germany

Supporting Information

ABSTRACT: Understanding interactions of bacterial surface polysaccharides with receptor protein scaffolds is important for the development of antibiotic therapies. The corresponding protein recognition domains frequently form low-affinity complexes with polysaccharides that are difficult to address with experimental techniques due to the conformational flexibility of the polysaccharide. In this work, we studied the tailspike protein (TSP) of the bacteriophage Sf6. Sf6TSP binds and hydrolyzes the high-rhamnose, serotype Y O-antigen polysaccharide of the Gram-negative bacterium *Shigella flexneri* (*S. flexneri*) as a first step of bacteriophage infection. Spectroscopic analyses and enzymatic cleavage assays confirmed that Sf6TSP binds long stretches of this polysaccharide. Crystal structure analysis and saturation transfer difference (STD) NMR spectroscopy using an enhanced method to interpret the data permitted the detailed description of affinity contributions and flexibility in an Sf6TSP-octasaccharide complex. Dodecasaccharide fragments corresponding to three repeating units of the O-antigen in complex with Sf6TSP were studied computationally by molecular dynamics simulations. They showed that distortion away from the low-energy solution conformation found in the octasaccharide complex is necessary for ligand binding. This is in agreement with a weak-affinity functional polysaccharide–protein contact that facilitates correct placement and thus hydrolysis of the polysaccharide close to the catalytic residues. Our simulations stress that the flexibility of glycan epitopes together with a small number of specific protein contacts provide the driving force for Sf6TSP-polysaccharide complex formation in an overall weak-affinity interaction system.

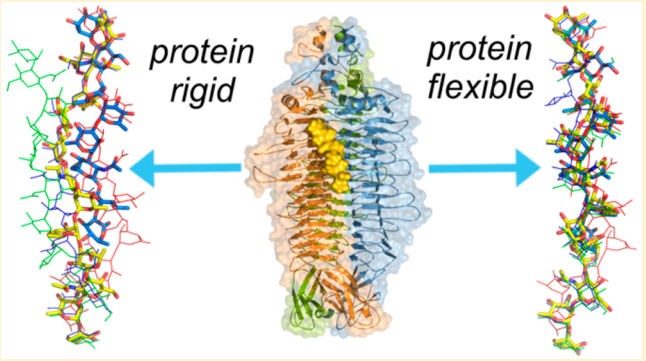

INTRODUCTION

In the bacterial cell, polysaccharide–protein interactions play a significant role from formation of structural components of the cell wall to functions in metabolic pathways. For example, polysaccharides interact with proteins of the bacterial glycan synthesis and the export apparatus transferring them to the outer membrane leaflet or into extracellular space.[1] Furthermore, polysaccharide–protein complexes are found in interactions with host immune systems,[2] during biofilm formation,[3] and in pathogenesis, which emphasizes the important role of bacterial polysaccharides as vaccine targets.[4] In contrast to their ubiquitous relevance in biology, descriptions of these complexes on a molecular level are scarce. Polysaccharide repeat units (RUs) in complex with antibodies have been analyzed with X-ray crystallography, molecular dynamics (MD) simulations and NMR spectroscopy.[5,6] The complex of a biofilm forming exopolysaccharide with a periplasmic transporter was characterized by X-ray crystallography and subsequent simulation of monosaccharide building blocks along an extended binding groove.[7] However, in most cases studied, rather short oligosaccharides (i.e., up to hexamers) were observed in direct contact to the protein, and so far only one decasaccharide and another dodecasaccharide complex have been described.[6,8] With growing chain length, the number of possible conformations increases quickly, and intramolecular H-bond formation may favor the occurrence of glycan secondary structure leading to a number of conformational epitopes.[9] Accordingly, the characterization of longer saccharide chains has to rely on a combination of experimental techniques and computer simulations.[10,11]

As part of the bacterial cell surface, polysaccharides are also a receptor for bacteriophages. Certain bacteriophages specifically recognize the O-antigen polysaccharide of Gram-negative

Received: January 8, 2016
Published: April 5, 2016

DOI: 10.1021/jacs.6b00240
J. Am. Chem. Soc. 2016, 138, 9109–9118

bacteria using tailspike proteins (TSP).[12] TSP attain specificity via long and shallow binding grooves, and several complexes of TSP with oligosaccharide fragments up to nonamer length have been described.[13−15] The Gram-negative bacterium *Shigella flexneri* (*S. flexneri*) causes bacillary dysentery with high mortality in infants in countries with low medical standards, and it therefore is an important vaccine target.[16] Most of the infective strains share a similar O-antigen with a polyrhamnose backbone. In this work, we have analyzed the binding of the O-antigen polysaccharide of *S. flexneri* to TSP of the bacteriophage Sf6 (Sf6TSP) to examine how extended polysaccharide chains interact specifically with a protein surface. The O-antigen consists of a carbohydrate backbone with high (75%) rhamnose content, and a growing body of evidence suggests that this specific composition gives rise to highly flexible, dynamic polymers.[17,18] Virulence of *S. flexneri* is intimately linked to this specific and dynamic O-antigen composition.[8,19] The basic unbranched serogroup Y antigen is composed of biological tetrasaccharide (ABCD) repeat units (RU) with the structure [→ 2)-α-L-Rha*p*-(1 → 2)-α-L-Rha*p*-(1 → 3)-α-L-Rha*p*-(1 → 3)-β-D-GlcNA*cp*-(1 →].[20] Sf6TSP recognizes specifically this O-antigen polysaccharide and cleaves the α-1,3 glycosidic bond between two rhamnose units, producing oligosaccharides (Scheme 1).[21,22] Sf6TSP

Scheme 1. Repeat Structure of *Shigella flexneri* Serogroup Y O-Polysaccharide Octasaccharide Obtained from Sf6TSP Cleavage[a]

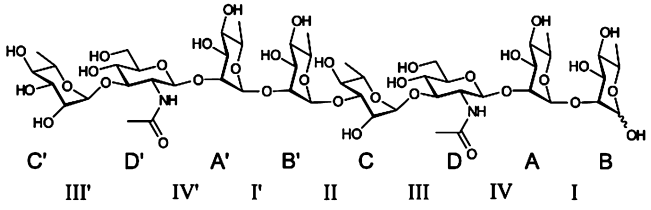

[a]Two repeat units of the *Shigella flexneri* O-serogroup Y polysaccharide antigen with the sequence [→ 3)-α-L-Rhap-(1 → 3)-β-D-GlcNAcp-(1 → 2)-α-L-Rhap-(1 → 2)-α-L-Rhap-(1 →]$_2$. Capital letters CDAB label monosaccharides, roman numerals glycosidic linkages as described elsewhere.[18]

forms a homotrimeric complex (M_W = 166 kDa) with a parallel β-helix architecture and three O-antigen binding sites located in long grooves at the subunit interfaces.[23] In the present work, we have analyzed Sf6TSP in the presence of polysaccharide fragments of different length and used a thorough experimental description as the starting point for computer simulations of long glycan fragments on the protein surface. We found that in the overall weak-affinity Sf6TSP polysaccharide interaction system specific protein contacts as well as the high flexibility of the binding partners are a prerequisite for complex formation.

RESULTS

Crystal Structure Analysis. Diffracting crystals were obtained for various complexes of Sf6TSP with octa-, dodeca- and lipopolysaccharides of *S. flexneri* O-serogroup Y. Only for the double mutant Sf6TSP E366A/D399A (Sf6TSP$_{mut}$), which is catalytically inactive[23] (Figure S1 in the Supporting Information), an octasaccharide ligand could be observed in the binding site (Figure 1A and Figure S2 in the Supporting Information) using a 1.95 Å resolution data set with space group P2$_1$ with six Sf6TSP$_{mut}$ chains per asymmetric unit (see

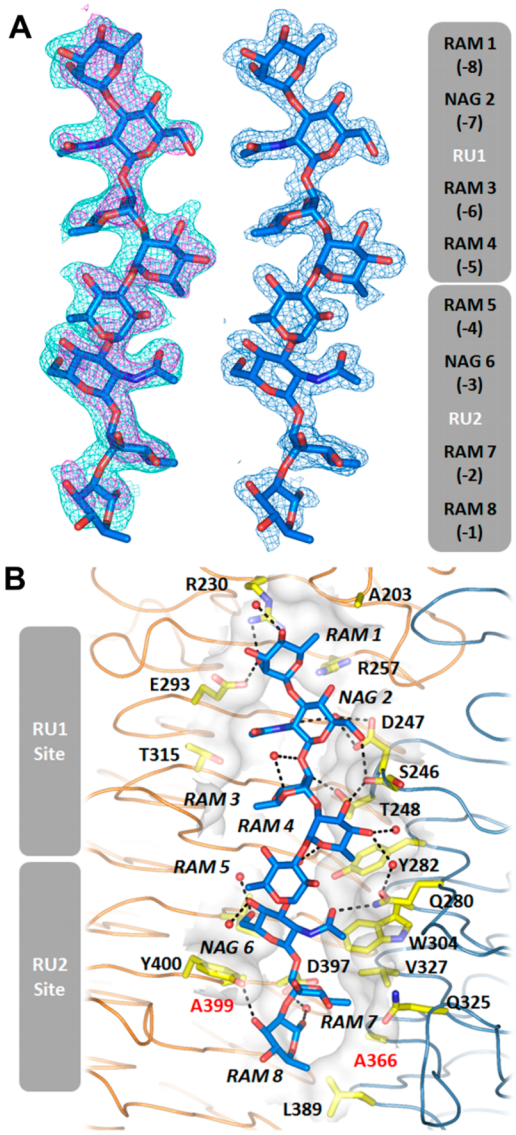

Figure 1. (A) Crystal structure of *Shigella flexneri* O-serogroup Y octasaccharide bound to Sf6TSP$_{Mut}$. (Left) Initial m|Fo|-D|Fc| electron density (red, 2.5 σ) and noncrystallographic-symmetry (NCS)-averaged m|Fo|-D|Fc| electron density (green, 2.0 σ). After refinement, six ligand molecules in the asymmetric unit superimposed with a root-mean-square deviation (rmsd) of 0.30 Å. (Right) 2m|Fo|-D|Fc| electron density (blue) after refinement (1.0 σ). The building blocks of RU1 and RU2 are defined as RAM (α-L-rhamnose) and NAG (N-acetyl-β-D-glucosamine). (B) Binding site of the Sf6TSP$_{Mut}$/octasaccharide complex between two subunits (orange and blue). RAM8 represents the reducing end of the octasaccharide. RU1 and RU2 sites mark the position of the repeating units 1 and 2, respectively, of the octasaccharide. Sixteen direct or water-mediated H-bonds are formed between ligand and protein. A366 and A399 are the mutated catalytic residues Glu and Asp, respectively.

Supporting Information for all crystallographic data). The previously described wild-type protein (Sf6TSP$_{WT}$) had been crystallized in space group R3 with one molecule per asymmetric unit.[23] Analysis of the atomic displacement factors (ADF) showed increasing flexibility of the monosaccharide units toward the reducing end, where in one of the octasaccharides the $^3S_1$ ring conformation was found for the terminal rhamnose instead of the anticipated $^1C_4$ conformation (see Figure S3 in the Supporting Information). The overall

DOI: 10.1021/jacs.6b00240
J. Am. Chem. Soc. 2016, 138, 9109−9118

architecture of ligand-bound Sf6TSP$_{mut}$ is identical with respect to ligand-free Sf6TSP$_{WT}$ (rmsd = 0.33 Å). The binding pocket of the Sf6TSP$_{mut}$-octasaccharide complex consists of a large groove formed by adjacent β-helix domains of different subunits in the trimer. The binding groove accommodates 2RU of O-antigen in the RU1 and RU2 sites (Figure 1B) flanked by the catalytic residues E366 and D399.[23] RU1 of the oligosaccharide forms a total of four direct H-bonds, seven water-mediated H-bonds, as well as three hydrophobic interactions with nine amino acid residues in total (RU1 site). RU2 follows the binding groove with fewer polar interactions than RU1 (two direct, three water-mediated H-bonds), but with three hydrophobic interactions (RU2 site). Overall, 15 ordered water molecules were found in H-bonding distance to the ligand.

NMR Studies of *S. flexneri* O-Serogroup Y Octasaccharide Bound to Sf6TSP. We analyzed the Sf6TSP$_{mut}$-octasaccharide complex in a 2D ^{1}H,^{1}H-trNOESY experiment (for the ^{1}H NMR characterization of the free ligand in solution see Table S3 in the Supporting Information). The bound octasaccharide showed the strongest interglycosidic cross-peaks from anomeric protons to protons on glycosyloxylated carbons (e.g., H2 or H3) for each glycosidic linkage (Figure 2A), as would be anticipated for an all-*syn* conformation.[24] Additional transglycosidic trNOEs were found between RAM5-H1 and NAG6-Ac, but not for the corresponding protons in RU1, which can be explained by a shorter distance between the spins in RU2. Likewise, a cross-peak was found in a spectral overlap region; due to its shape it was assigned to a correlation between the methyl group in NAG2-Ac and RAM1-H2. For RU2 the corresponding cross-peak was missing. These results are in agreement with a change between the ϕ1 and ϕ5 torsion angles of 9−15° as well as 15−20° for the ψ1 to ψ5 torsion angles, as seen in the crystal structure and in the MD simulations (see below and Supporting Information). The *N*-acetyl groups also show transglycosidic trNOEs to the H4 protons of RAM3 and RAM7. Furthermore, trNOEs were observed for the methyl groups of RAM3, RAM7 and RAM4 to RAM4-H1, RAM8-H1 and RAM5-H2. Together with the absence of transglycosidic trNOEs from any of the methyl groups of RAM1 and RAM5, all results from trNOESY-NMR are in good agreement with the bound octasaccharide conformation seen in the crystal structure. ^{1}H saturation transfer difference (STD) NMR experiments were performed (Figure 2B) and initial slopes of STD amplification factor build up curves (STD-AF$_0$) were calculated (see tabulated values in the Supporting Information). The methyl group of RAM4 has the highest STD-AF$_0$ when saturating aromatic protein residues, which is in agreement with the crystal structure where it is buried in the protein in close proximity to Tyr282. The second strongest STD-AF$_0$ is the average of RAM3-H4 and RAM7-H4, of which the latter is adjacent to Trp304. The absence of aromatic residues is more profound at the nonreducing end of the binding pocket, and this is reflected in the lower STD-AF$_0$ values for NAG2-Ac compared to NAG6-Ac. A particularly weak STD-AF$_0$ found for RAM5 may be explained by a longer distance to the protein surface for this residue due to the pucker in the saccharide chain (see Figure S4 in the Supporting Information).

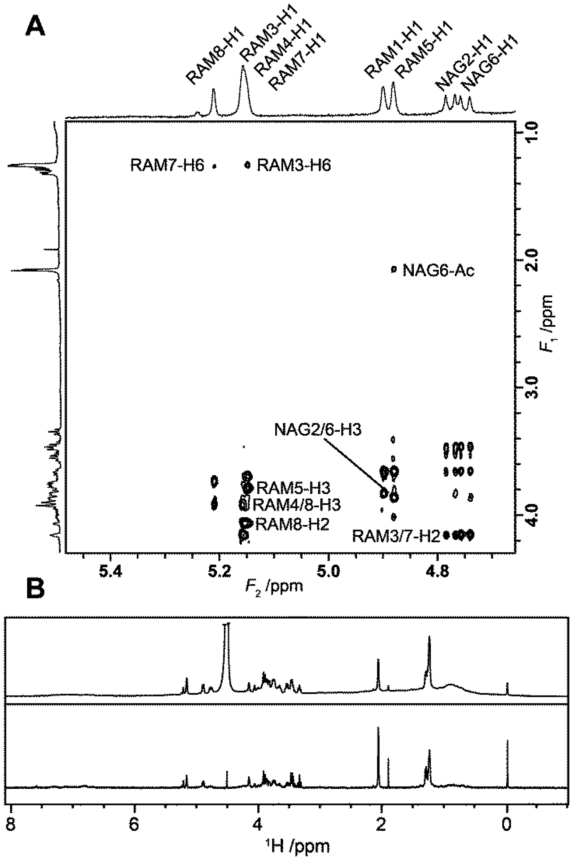

Figure 2. (A) ^{1}H,^{1}H-trNOESY spectrum with selected interglycosidic cross-peaks annotated. (B) ^{1}H NMR spectrum (top) and an STD spectrum (bottom) of Sf6TSP with the octasaccharide in D_2O. The irradiation frequency in the STD experiment was set to 7 ppm, and the saturation time was 2 s.

Molecular Dynamics Simulations. We started simulations of Sf6TSP in complex with tetrasaccharide fragments (Figure 3A), with the protein kept at the geometry of the X-ray structure. During MD runs of at least 100 ns length, tetrasaccharides remained stable in the RU1 site, reproducing the binding mode found in the crystal structure including some of the structural water molecules.[23] The bound tetrasaccharide assumes the solution conformer close to the global free-energy minimum. Also, an octasaccharide resided stably in the binding site during MD simulations, both in the Sf6TSP$_{WT}$ and Sf6TSP$_{mut}$ in a conformation similar to that observed in the X-ray structure (Figure 3B). The H-bond pattern found in the crystal structure was well reproduced showing that the octasaccharide was mainly fixed in the binding site via RAM1, RAM3 and RAM8. Average torsion angles within RU1 of the bound octasaccharide settle in the same energy minima as in RU2 (Figure 3C and Tables S5 and S6 in the Supporting Information). Rmsd values of monosaccharide positional variations increased from 0.9 Å at the nonreducing end to 2.6 Å at the reducing end in agreement with increased atomic displacement factors found in the crystal structure.

Simulation of STD-NMR Build-up Curves Using a Novel Modified CORCEMA Approach Accounting for Chemical Shift Dispersion (CSD) in Large Proteins. In order to further validate the X-ray and computational protein−ligand models we simulated STD-AF build-up curves by employing a complete relaxation and conformational exchange matrix (CORCEMA).[25] Sf6TSP is a trimeric protein complex with a molecular weight of 166 kDa. To describe the magnetic saturation of this large protein−ligand complex accurately, the chemical shift dispersion (CSD) caused by rapid transverse relaxation had to be considered. In the resulting CORCEMA-

DOI: 10.1021/jacs.6b00240
J. Am. Chem. Soc. 2016, 138, 9109−9118

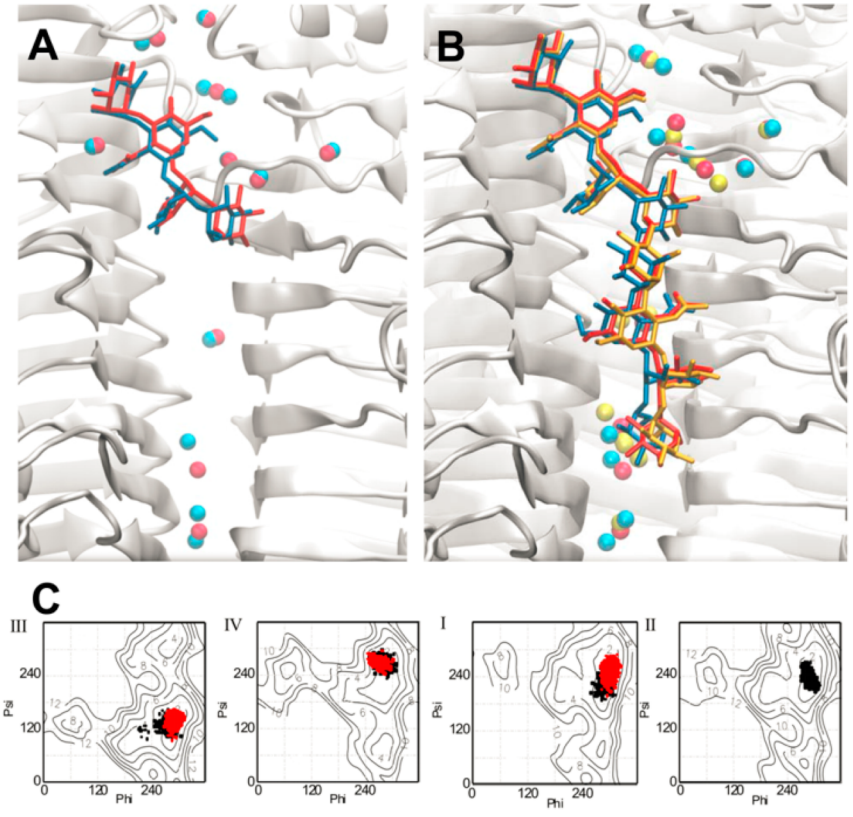

Figure 3. MD simulations of Sf6TSP oligosaccharide complexes obtained with Glycam/Amber force fields. (A) Tetrasaccharide complex with Sf6TSP wild type (red) in comparison with position in the crystal structure (blue; pdb: 2VBM). (B) Octasaccharide complex with Sf6TSP wild type (red) or mutant E366A/D399A (yellow) in comparison with position in the crystal structure of the mutant E366A/D399A (blue; pdb: 4URR). (C) $\phi-\psi$ distributions of the octasaccharide bound to Sf6TSP. Black and red dots represent the $\phi-\psi$ distributions of the RU1 and the RU2 site, respectively. Free energies were calculated for linkages I,II, III and IV (cf. Scheme 1) in disaccharides as described previously.[18] Linkage II is only present in the octasaccharide. For a comparison of torsion angle distributions see Table S5 in the Supporting Information.

ST-CSD approach the NMR line shapes influenced by the transverse relaxation time T_2 were taken into account by looping the CORCEMA-ST program for narrow intervals (n) over the whole spectrum. Concomitantly, relative contributions to the spectral intensity within the defined irradiation bandwidth ($X_{sat,n}$) were calculated for protons in the binding site and with chemical shifts within an interval n (Scheme 2; for full description of the CORCEMA-ST-CSD analysis see the Supporting Information). The simulated CORCEMA-ST output for each interval n (STD-AF$_{CORCEMA\text{-}ST,n}$) was multiplied with the corresponding $X_{sat,n}$ and the sum over all n reported as the final simulated result (STD-AF$_{sim}$, eq 1).

$$\text{STD-AF}_{sim} = \sum_{n=1}^{N} X_{sat,n} \cdot \text{STD-AF}_{CORCEMA\text{-}ST,n} \quad (1)$$

Simulated STD-AF showed good agreement with experimental values when the average ligand atomic coordinates from the MD trajectory were evaluated with an R_{NOE} between 0.32 and 0.53. When using the ligand model from the crystal structure, good agreement with the experiment was only found for STD-AF$_{sim}$ from resonances at the nonreducing end (Figure 4A). By contrast, STD-AF$_{sim}$ of RAM8 deviated from experimental STD-AF significantly (Figure 4B). These results emphasize the dynamic nature of the reducing end and show that MD simulations fully accounted for the octasaccharide dynamics experimentally observed in the binding site, whereas the crystal structure accounted for the observed reducing end flexibility only by showing increased atomic displacement factors.

Determinants of Affinity in the Sf6TSP Binding Site. Aromatic as well as glutamate residues near the ligand are underrepresented in Sf6TSP when compared with rhamnose- or *N*-acetylglucosamine-binding proteins (see Figure S10 in the Supporting Information). Together with the small number of

Scheme 2. CORCEMA-ST-CSD Approach[b]

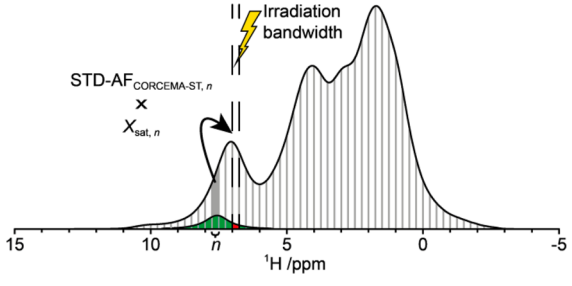

[b]The concept of the CORCEMA-ST-CSD approach. The spectrum is divided into separate regions (n) and for each one a CORCEMA-ST simulation is performed to generate a set of STD-AF$_{CORCEMA\text{-}ST,n}$. Each region is then multiplied with $X_{sat,n}$, i.e., the part of the chemical shift distribution for the specific region that is within the irradiation bandwidth (the red area) divided with full distribution (the sum of the red and green areas). The final STD-AF$_{CSD}$ is calculated as the sum of all STD-AF$_{CORCEMA\text{-}ST,n}$ in the spectrum.

DOI: 10.1021/jacs.6b00240
J. Am. Chem. Soc. 2016, 138, 9109−9118

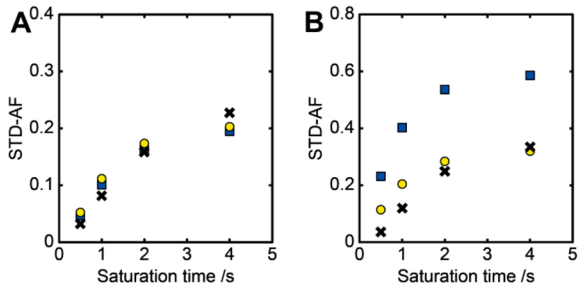

Figure 4. CORCEMA-ST-CSD simulated STD-AF for RAM1-H1 (A) or RAM8-H1 (B) anomeric resonances. Ligand coordinates used from molecular dynamics simulations (yellow circles) and X-ray ligand B (blue squares) compared to experimental STD-AF (crosses).

ligand-protein contacts observed this points to low octasaccharide affinity. In fact, attempts to quantify the affinity of complex formation with isothermal titration calorimetry failed and we could only estimate the dissociation constants for the Sf6TSP-octasaccharide complex to lie in the mM range. Using docking, the binding poses from X-ray analysis were recognized as low-energy (Figure 5A). Potential of mean force calculations by umbrella sampling showed that energies needed to pull tetra- or octasaccharides out of their binding sites agreed well with the free energies obtained from docking, which illustrates

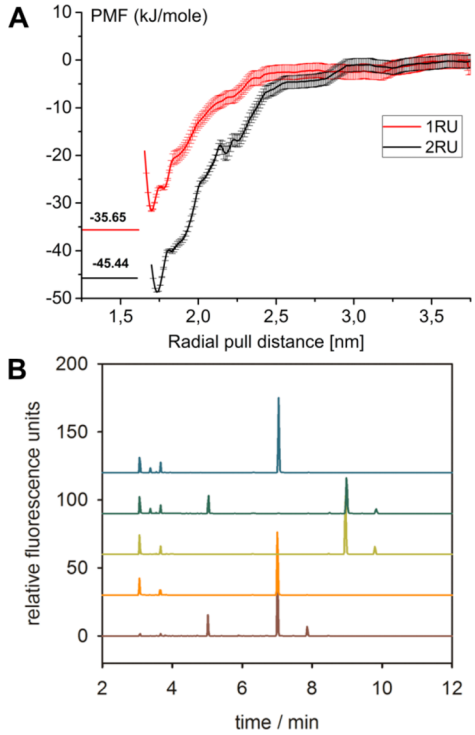

Figure 5. (A) Potential of mean force (PMF) curves for tetrasaccharide (red) and octasaccharide (black) Sf6TSP complex formation. As reference the highest scores obtained by docking are given as horizontal lines in kJ mol^{-1}. (B) Sf6TSP cleavage products of *S. flexneri* serogroup Y oligosaccharides or lipopolysaccharide (LPS). Samples were analyzed by capillary electrophoresis with laser-induced fluorescence detection (CE-LIF) after fluorophore labeling. From bottom to top: LPS cleavage products, octasaccharide control, dodecasaccharide control, dodecasaccharide with fluorescence label at the reducing end incubated with Sf6TSP, octasaccharide incubated with Sf6TSP.

that adding the second repeat unit increased the binding affinity only moderately. This agrees with the finding that the H-bond network fixing the octasaccharide in the Sf6TSP binding groove is mainly located at the RU1 site. Mutation of residues in the RU1 site drastically increased octasaccharide flexibility in the binding groove and illustrates its important role in generating specificity (Figure S11 in the Supporting Information). Given that the catalytic residues are located at the C-terminal end of the binding groove next to the RU2 site, this binding mode must also influence the size of polysaccharide cleavage products. After Sf6TSP$_{WT}$ lipopolysaccharide (LPS) hydrolysis we indeed only found the octasaccharide as the main product (Figure 5B), in agreement with at least the RU1, RU2 and an additional RU3 site occupied during cleavage. By contrast, starting with octasaccharide as educt, it was not cleaved into tetrasaccharides, even after several days of incubation with Sf6TSP, whereas tetrasaccharides could be produced from the dodecasaccharide.[22] This further corroborates that also the RU2 site has to be occupied for successful cleavage and also contributes to substrate affinity.

Binding Studies of Sf6TSP with Long O-Antigen Fragments. Polysaccharide interactions of Sf6TSP were analyzed on surface-immobilized LPS preparations of *S. flexneri* serogroup Y with surface plasmon resonance (Figure 6A). To

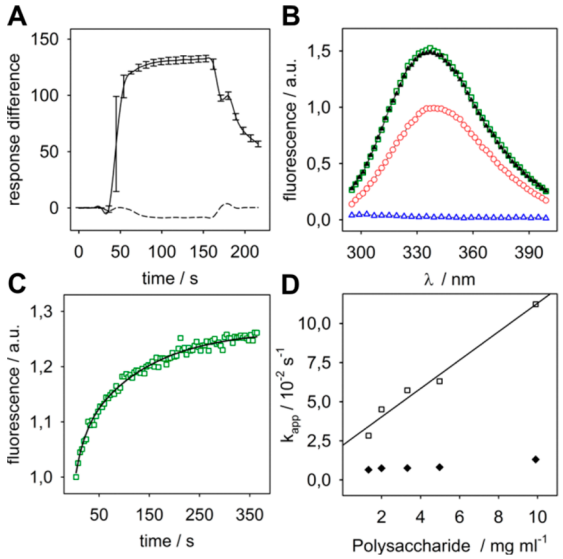

Figure 6. *S. flexneri* serogroup Y polysaccharide binding to Sf6TSP. (A) Surface plasmon resonance (SPR) response upon binding of Sf6TSP (100 μg mL^{-1}) of cleavage-deficient mutant D399A to immobilized LPS (solid) or to immobilized LPS enzymatically pretreated with Sf6TSP$_{WT}$ (dashed). Error bars represent standard deviations from three injections at 25 °C. (B) Normalized protein fluorescence spectra of 184 nM Sf6TSP E366A/D399A in the absence (red open circles) or presence of 33.2 μg mL^{-1} (green open squares) or 66.2 μg mL^{-1} (filled black triangles) polysaccharide. Control: 66.2 μg mL^{-1} polysaccharide without protein (open blue triangles). (C) Relaxation to binding equilibrium at 10 °C upon manually mixing 184 nM Sf6TSP E366A/D399A with 33.2 μg mL^{-1} polysaccharide (open green squares) described by a biexponential model with k_1 = 5.73 ± 0.94 × 10^{-2} s^{-1} and k_2 = 0.76 ± 0.04 × 10^{-2} s^{-1} (solid line). (D) Concentration dependence of apparent rate constants k_{app} of slow (filled diamonds) and fast (open squares) kinetic phases. A polysaccharide dissociation rate constant of 0.022 ± 0.003 s^{-1} was determined from the linear fit of the fast phase as described elsewhere.[26]

DOI: 10.1021/jacs.6b00240
J. Am. Chem. Soc. 2016, 138, 9109−9118

prevent polysaccharide cleavage, the catalytically inactive Sf6TSP D399A mutant was used. The protein specifically bound to long O-antigen chains, but was unable to recognize LPS preparations that were pretreated enzymatically with $Sf6TSP_{WT}$ to cleave off the O-polysaccharide from the surface. We can therefore exclude that LPS core- or lipid A-moieties interact with Sf6TSP. Rather, the long O-antigen chains on intact LPS are required for stable interaction. Moreover, dissociation off-rates from the LPS surface were comparable to those measured as protein fluorescence signal relaxation rates obtained upon manual mixing with polysaccharide preparations of different concentrations (Figures 6B–D and Figure S12 in the Supporting Information). Off-rates of similar magnitude were also found for dissociation of a *Salmonella* O-antigen polysaccharide from bacteriophage P22TSP.[12]

To obtain a molecular description of a Sf6TSP binding mode for ligands longer than an octasaccharide we extended our MD analysis to dodecasaccharides to explore possible binding modes of longer chains. We simulated a fragment of three RUs by extending the octasaccharide by another repeating unit into a putative RU3 site located beyond the catalytic residues. However, simple extension of the octasaccharide by another RU while keeping its initially bound position and staying close to a minimum-energy conformation was hindered by steric clashes (see Figure S13 in the Supporting Information). To avoid the latter, a high-energy starting conformation was chosen with RU3 rotated around linkage II into a state of torsion about 7 kcal mol^{-1} above the global minimum for that linkage.[18] Irrespective of whether the Glycam/Amber or the CHARMM force field was used, in subsequent MD runs all glycosidic torsions rapidly adjusted within 10 ps to low energy conformations. As initial result, the dodecasaccharide settled in an elongated pose into the binding groove for a period of up to 10 ns. However, during the further simulation time RU1 and RU2 permanently detached from the octasaccharide binding site (Figure 7A). With Glycam/Amber, RU1 and RU2, although displacing, stayed in contact with the TSP surface, whereas RU3 was fixated from the beginning through H-bonds between Asn455 and RAM11, Arg364 and NAG10, and RAM12 and Asn508, respectively. In the CHARMM case, the dodecasaccharide eventually left the groove and temporarily was even seen to detach from the TSP surface (see Figures S14 and S15 in the Supporting Information for all simulations). Furthermore, in a second set of simulations, we enhanced protein flexibility and released all restraints from the protein backbone in the β-strand-connecting loops. This seems a reasonable assumption for the protein dynamics at ambient temperature, and all subsequent simulations showed that this did not affect the global shape of Sf6TSP as all protein C-α positions stayed close to those found in the crystal structure. Using Glycam/Amber, the dodecasaccharide now quickly relaxed into an elongated pose with its first two RUs largely following the orientation of the octasaccharide in the crystal structure (Figure 7B), whereas RU3 took a similar position to that seen in the simulations with restrained loop backbones but with more stably occupied H-bonds (Figure 7D and Table S6 in the Supporting Information). Also in the CHARMM simulations with flexible loops the ligand was firmly accommodated along the groove, but showed more conformational flexibility than in the Glycam/Amber simulations (Figure 7C). Especially RU3 was still dynamically moving back and forth between the two walls of the binding groove, as also illustrated by a lower H-bond occupancy (expressed through

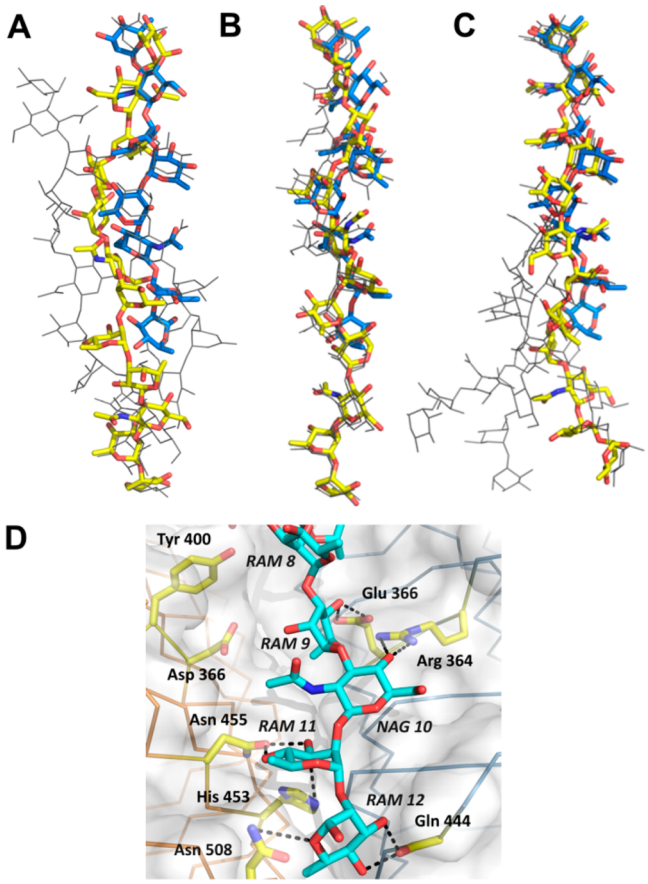

Figure 7. Superimposition of *S. flexneri* serogroup Y octasaccharide model in complex with Sf6TSP from the crystal structure (blue) with final poses of dodecasaccharide after 100 ns of molecular dynamics simulation (yellow) obtained with different force fields. (A) Glycam/Amber, protein backbone restrained (gray: snapshots at 35 and 60 ns) (B) Glycam/Amber, protein loops unrestrained (gray: snapshots at 22 and 60 ns) (C) CHARMM, protein loops unrestrained (gray: snapshots at 15, 20, and 25 ns). (D) Binding site of RU3 in the Sf6TSP-dodecasaccharide complex between two subunits (orange and blue) shown for the Glycam/Amber unrestrained protein backbone simulation. For more MD snapshots and all trajectories of the simulations see the Supporting Information.

average acceptor-donor distances, see Figure S14 and Table S6 in the Supporting Information).

DISCUSSION

Sf6TSP as an Example for Weak-Affinity Polysaccharide Binding. Carbohydrate ligands become more flexible with increasing length, resulting in weak affinities challenging the understanding of how polysaccharides bind to proteins transiently. For example, in processes such as polysaccharide synthesis and hydrolysis,[27] chain length control[28] or transport,[29] short-lived polysaccharide binding may take place with rapid ligand off-rates. The computational approach fills the gap between the experimentally accessible descriptions of small oligosaccharides in protein binding sites and the need for models of large protein–polysaccharide complexes.[10,30] The Sf6TSP analyzed in this work is a polysaccharide hydrolyzing enzyme. It recognizes and cleaves the specific O-antigen part of LPS as the first step of the bacteriophage Sf6 infection cycle in order to penetrate the protective polysaccharide coat of the bacteria and reach outer membrane receptors.[31] The

DOI: 10.1021/jacs.6b00240
J. Am. Chem. Soc. 2016, 138, 9109–9118

bacteriophage is equipped with six TSP and hence displays 18 polysaccharide binding sites to ensure multivalent fixation on the bacterial cell surface, whereas TSP hydrolysis and rebinding enable receptor search and lateral movement of the phage across the membrane LPS layer. The Sf6TSP glycan binding groove only offers a limited number of H-bonding contacts providing specificity while hydrophobic patches are lacking, resulting in an overall weak-affinity polysaccharide interaction system.

Experimental and Computational Methods to Describe Glycan Ligand Flexibility in Sf6TSP Complexes. Sf6TSP-octasaccharide complexes showed flexibility at the glycan reducing end. In many cases, ligand flexibility is not well resolved in crystal structures due to averaging over atom positions by crystallographic symmetry. Also in a previous study, electron density was only found for the tetrasaccharide in the RU1 site when $Sf6TSP_{WT}$ crystallized in a space group of higher symmetry.[23] However, the $Sf6TSP_{Mut}$ octasaccharide complex forms a crystallographic asymmetric unit with two TSP trimers. This produced six distinct snapshots of ligand conformations preserved upon cooling from ambient to cryo temperatures and thus captured the flexibility of the octasaccharide reducing end. MD simulations in combination with build-up rates found with STD-NMR at 56 °C provided a dynamic picture of this flexibility. Nevertheless, a potential difficulty with this and NMR analyses in general is that polysaccharide binding may involve large interaction surfaces. The analysis of high molecular weight protein−ligand complexes sets limits to quantitative STD-NMR analyses in cases where the irradiation frequency interval does not fully cover the chemical shifts of certain protein resonances, resulting in only partially saturated signals. Yet, the simulation of STD-AF build-up curves with classical CORCEMA-ST relies on precise chemical shifts.[25,32] Predicting chemical shifts computationally is sometimes inaccurate; however, in the expanded CORCEMA-ST-CSD approach used in this work to analyze STD data from Sf6TSP-oligosaccharide complexes, chemical shifts are described as distributions rather than as discrete signals and thus are less sensitive to the chosen irradiation interval in the corresponding simulation. In addition, all results were calculated directly from estimated physical parameters (e.g., $\tau_{C\text{-protein}}$, $\tau_{C\text{-ligand}}$, K_D, etc.) without any major parameter optimization. This is in contrast to the high number of input parameters used in CORCEMA-ST that may result in forced fitting scenarios. Hence in the present study, NMR spectroscopy and X-ray crystallography provided robust validation of the computational descriptions of TSP O-antigen binding. This emphasizes the improvement in the quality of carbohydrate force fields due to specifically adapted glycan parametrization procedures.[33,34] MD simulations in this study showed good agreement of water positions with those in the crystal structure (cf. Figure 3). However, the fundamental challenge remains in assigning desolvation penalties to individual water molecules in order to predict binding affinities from simulation data.

Computational Simulation of Binding of Long Polysaccharide Fragments to Sf6TSP. In this work, the thorough experimental description of octasaccharide binding to Sf6TSP and the excellent agreement with data from MD simulations is prerequisite for the definition of a plausible computational setup that finds binding modes of dodecasaccharide fragments. It should be emphasized that no experimental evidence of a dodecasaccharide pose is yet available; soaking of Sf6TSP crystals with dodecasaccharide, polysaccharide or lipopolysaccharide, for instance, had not shown any interpretable ligand electron density, as ligand flexibility is likely to cause disorder in the crystal. For the octasaccharide ligand, the experiments clearly emphasized the enhanced flexibility of RU2. This suggests that RU2 and RU3 have enough freedom to adapt their conformation while choosing a high energy dodecasaccharide starting conformer that avoids steric clashes. At the same time, fixing RU1 in the RU1 site is required. This finding is corroborated by the observation that mutations of H-bond providing residues E293 and D247 in the RU1 site had previously shown a reduced hydrolysis turnover,[23] stressing that the corresponding protein−ligand H-bonds are important to position the polysaccharide fragments correctly for cleavage. In the computational setup, the backbone of the protein loops had to be made fully flexible to establish all contacts in the −2 site correctly, whereas contacts in site +1 were similar irrespective of protein loop flexibility. In combination with a high-energy dodecasaccharide starting conformer in the simulation this helps to overcome local barriers presented by the protein scaffold and to sample conformations slightly elevated in energy in order to arrive at the final pose.

With essentially a single, albeit plausible high energy starting conformation the sampling of possible final dodecasaccharide poses cannot be expected to be exhaustive, and the assignment of initial conditions is currently a limitation of our study. However, the MD simulations calculated with either the CHARMM or Glycam/Amber force field produced rather similar results especially with respect to the octasaccharide binding mode or in predicting its dynamics at the reducing end. The spread in H-bond occupancies and distances may be seen in analogy to the experimental uncertainty. Thus, from the combined results of the two force fields used we obtain a reasonable and broad variation of poses for the dodecamer that are well compatible with the placement of the octasaccharide, i.e. the first two RUs. Compared to Glycam/Amber, CHARMM based simulations in general suggested enhanced ligand dynamics, especially for RU3. Moreover, in case of Sf6TSP, releasing restraints from loop backbone carbon atoms was essential to obtain a reasonable glycan conformational ensemble with respect to the crystal structure. In addition, also ligand flexibility was needed as shown by a control simulation with RAM1 fixed to its position in the RU1 site. In this case the ligand was unable to find an overall stable binding pose within the given simulation time (Figure S16 in the Supporting Information). Whereas the Sf6TSP-octasaccharide complexes analyzed in this work comply very well with the general observation that glycan low-energy solution conformers are recognized, the MD simulations of the dodecasaccharide complex showed that the conformation of the octasaccharide subunit (RU1 and RU2) is slightly distorted, with standard deviations of the fluctuations in all glycosidic angles notably increased (cf. Table S5). It is therefore not surprising that in the present case both, the ligand and the protein must provide flexibility to correctly place the polysaccharide in the Sf6TSP catalytic site for cleavage. The accommodation of the dodecasaccharide may eventually be understood with a progressive conformational binding model,[35] with a relaxation pathway leading through a rugged energy landscape. Finally, Glycam/Amber simulations suggested that glycan-protein contacts were mainly established by RU1 and RU3, positioning RU2 favorably for catalytic attack, whereas CHARMM simulations with enhanced flexibility in the binding groove

DOI: 10.1021/jacs.6b00240
J. Am. Chem. Soc. 2016, 138, 9109−9118

showed these substrate contacts as being more transient. This again emphasizes that octasaccharide binding to sites RU2 and RU3 alone is unlikely and that dodecasaccharides are the minimal substrates, in agreement with the experimental results.[22] Whether or not a stable pose as predicted by Glycam/Amber is a prerequisite for cleavage can ultimately only be answered by quantum chemical approaches such as QM/MM simulation techniques.

In summary, the approach used in this study, to experimentally establish a precise picture of not only glycan−protein interactions, but also glycan dynamics in the binding site could be a valuable scheme in other cases of weakly binding polysaccharide−protein complexes, where the extrapolation toward long polysaccharide fragments with computational methods is desired.

METHODS

Materials. All experiments were carried out with N-terminally shortened TSP lacking the capsid adaptor domains (Δ*N*, residues 109−622, M_W = 166 kDa for the native trimer).[22] LPS, polysaccharide and oligosaccharides of *S. flexneri* O-serogroup Y were obtained from Nils Carlin (Scandinavian Biopharma) and purified as described.[36]

Crystallization, Data Collection and Structure Determination. The complex of Sf6TSP E366A/D399A and octasaccharide (2RU) crystallized in space group $P2_1$ at room temperature by sitting-drop vapor-diffusion mixing 3 μL of protein solution (10 mg/mL in 10 mM sodium phosphate pH 7.5) with an equal volume of precipitant solution (0.1 M MES pH 6.5, 20 mM $MnCl_2$, 16 % w/v PEG 8000) and 0.6 μL of octasaccharide (15 mM in H_2O). Crystals appeared within 2 weeks, were transferred into cryo-protectant (0.1 M MES pH 6.5, 20 mM $MnCl_2$, 25 % w/v PEG 8000, 15 % w/v ethylene glycol) and frozen in liquid nitrogen. A 1.95 Å resolution data set was collected at 100 K at BL14.1 operated by the Helmholtz-Zentrum Berlin (HZB) at the BESSY II electron storage ring[37] and processed with XDS[38] and POINTLESS.[39] The crystal showed nonmerohedral twinning (twinning fraction α = 0.28) and in addition, noncrystallographic translational symmetry (NCS). Initial phases were obtained by molecular replacement with Phaser[40] from the CCP4 suite[41] using the nonisomorphous structure (space group R3) of wild-type Sf6TSP bound to tetrasaccharide[23] (PDB: 2VBM). In order to minimize model bias, the initial polyalanine model with six copies of Sf6TSP per asymmetric unit was automatically rebuilt using ARP/WARP.[42] Iterative cycles of interactive model building with COOT[43] and refinement with REFMAC5[44] and BUSTER[45] led to the final model statistics (summarized in Table S2 of the Supporting Information). Geometrical restraints used during refinement of the oligosaccharide and solvent molecules were generated with the GRADE web server (http://grade.globalphasing.org, Global Phasing Ltd.). Quality Control Check v3.0 was used for validation of the model (http://smb.slac.stanford.edu/jcsg/QC/, Joint Center for Structural Genomics). Two trimers, the functional Sf6TSP quaternary structure, were found to be generated by NCS from all six protein chains in the asymmetric unit with an rmsd of 0.22 Å for all Cα atoms. The final model coordinates have been deposited at the Protein Data Bank with accession number 4URR. Figures were generated with PyMOL.[46]

NMR Spectroscopy. NMR chemical shift assignment, ^{1}H T_1 spin relaxation, ^{1}H,^{1}H transfer NOESY (trNOESY) and ^{1}H saturation transfer difference (STD) NMR experiments were performed at 56 °C on a 500 MHz Bruker Avance NMR spectrometer equipped with a TCl-Z-Gradient cryoprobe. Sf6TSP keeps its native fold at 56 °C (see Figure S17 in the Supporting Information). For octasaccharide shift assignment see Table S3. The ^{1}H,^{1}H trNOESY and ^{1}H STD NMR experiments were performed on a sample containing Sf6TSP D399N (0.12 mM) and the octasaccharide ligand (1.87 mM) in D_2O sodium phosphate buffer (100 mM, pD = 7). The 2D ^{1}H,^{1}H transfer NOESY spectrum was recorded using a phase-sensitive pulse sequence[47] with a calibrated zero quantum suppression filter[48] and a mixing time of 120 ms. A reference experiment on a sample of the ligand per se was performed to ensure the absence of NOE for the ligand in solution at this temperature.[49] Four ^{1}H STD experiments[50] were acquired with different saturation times (0.5, 1, 2, and 4 s). Saturation of the protein was achieved by irradiating on-resonance at either 7.0 or −0.4 ppm with a pulse train of 50 ms Gaussian pulses using a power level corresponding to a hard square pulse of 24 Hz; the same pulse train was irradiated off-resonance at 60 ppm as reference. STD amplification factors (STD-AF)[51] were calculated, and STD build-up curves were fitted exponentially to obtain STD-AF_0. The CORCEMA-ST-CSD analysis was conducted by altering the irradiation frequencies in intervals of 0.05 ppm using the CORCEMA-ST program.[25,52] Parameters employed in the CORCEMA-ST simulations were used as initially estimated; a free ligand correlation time of 253 ps calculated from the pulsed field gradient diffusion measurements, a correlation time of 23.9 μs when bound was calculated from the molecular mass of the protein as a trimer (166 kDa), an internal correlation time being 1 order of magnitude shorter,[53] i.e., 25.3 ps, an order parameter of 0.85,[54] estimated K_A = 2000 M^{-1}, k_{on} = 1 × 10^7 s^{-1} M^{-1}, an active-site cutoff of 6 Å and ρ_{leak} = 0.1 s^{-1}. Chemical shifts of the protein in the X-ray and MD molecular models were estimated by using the ShiftX2 software,[55] using the ShiftY addition. In cases where the chemical shifts were not predicted by the ShiftX2 calculation, they were estimated using the predicted chemical shift of a neighboring spin. The missing chemical shift of spin *i* was calculated as $\delta_{calc,i} = \bar{\delta}_i + \sigma_i(\delta_{calc,j} - \bar{\delta}_j)/\sigma_j$ where $\delta_{calc,j}$ is the predicted chemical shift of the neighboring spin, $\bar{\delta}$ is the average chemical shift and σ the standard deviation of a specific atom in an amino acid (data taken from the BMRB database).[56] The transverse relaxation time ($T_{2,protein}$) of Sf6TSP was estimated to 3.85 ms from a ^{1}H spectrum simulation based on the ShiftX2 chemical shifts of Sf6TSP.

Sf6TSP Polysaccharide Interaction Analyses. LPS preparations were immobilized, and surface plasmon resonance experiments were carried out as described.[57] Protein fluorescence was measured on a Fluoromax 3 spectrofluorimeter (HORIBA Jobin Yvon, Bensheim, Germany) in poly(methyl methacrylate) (PMMA) cuvettes in 50 mM sodium phosphate buffer pH 7 at 184 nM TSP concentration in 3 mL test volume at 10 °C, with λ_{Ex} = 280 nm. Spectra were corrected for dilution upon polysaccharide addition. Polysaccharide binding kinetics were monitored at λ_{Em} = 336 nm, traces were fitted with a biexponential fit and k_{diss} obtained from apparent rate constants k_{app} using the relationship $k_{app} = k_{diss} + k_{ass} \cdot (c_{Polysaccharide} + c_{TSP})$ as described elsewhere.[26] The polydisperse nature of polysaccharide prevented calculation of molar concentrations and thus of k_{ass} from the data. For cleavage product analysis, 1 mg/mL LPS was incubated with 20 μg/mL Sf6TSP for 6 days at room temperature and precipitated with 80 % (v/v) ethanol. The dried supernatant or the respective octa- or dodecasaccharide controls were dissolved in 2 μL 8-aminopyrene-1,3,6-trisulfonic acid (200 mM in 15% (v/v) acetic acid) and 2 μL sodium cyanoborohydride (1 M in tetrahydrofuran), incubated overnight at 37 °C and diluted with 96 μL water. Samples were diluted 400-fold and subjected to capillary electrophoresis as described elsewhere.[58]

Theory. All molecular dynamics (MD) simulations were carried out using the Amber force field ff03[59] in combination with the GLYCAM parametrization for carbohydrates[33] and CHARMM36 with an improved set of carbohydrate parameters.[34,60] MD simulations were conducted in GROMACS with the TIP3P water model.[61] Molecular topology and coordinate files for the carbohydrate were created with AmberTools using tLeap as part of Amber11,[62] and then translated to GROMACS input files via a modified amb2gmx.pl.[63] After an equilibration phase, production runs between 100 and 200 ns duration at constant volume were carried out using a velocity-Verlet integrator with half-step averaged kinetic energies and a time step of 2 fs. The temperature of 310 K was maintained with a multichain Nose-Hoover thermostat.[64] The particle mesh Ewald (PME) method was used to calculate electrostatic interactions with a cutoff of 1.2 nm for the separation of the direct and reciprocal space summation.[65] H-bonds within water were treated with the SETTLE algorithm,[66] other constraints were treated with LINCS.[67] Docking was carried out with

DOI: 10.1021/jacs.6b00240
J. Am. Chem. Soc. 2016, 138, 9109−9118

Autodock v. 4.2.[68] Initial coordinates were obtained from the averaged saccharide structures after MD simulation with ϕ glycosidic torsions set as rigid in order to obtain rational saccharide conformations, and 100 runs were performed for each docking trial. Binding free energies were determined with the umbrella pulling procedure implemented in GROMACS as an application of the weighted histogram analysis method.[69]

■ ASSOCIATED CONTENT

Supporting Information

The Supporting Information is available free of charge on the ACS Publications website at DOI: 10.1021/jacs.6b00240.

Crystal structure analysis data, analyses of catalytic activity of Sf6TSP$_{Mut}$, NMR chemical shift assignments, STD-AF$_0$ data, the CORCEMA-ST-CSD approach, binding site analysis with GlyVicinityDB, CD and fluorescence spectra, torsions in the simulation start structure, rmsd traces and snapshots of MD simulations, glycosidic torsion angles and H-bonds from molecular dynamics simulations. (PDF)

■ AUTHOR INFORMATION

Corresponding Authors

*mark.santer@mpikg.mpg.de
*barbirz@uni-potsdam.de

Present Addresses

[#]College of Pharmaceutical Sciences, Zhejiang University, Hangzhou, Zhejiang 310058, PR China.
[∇]University of Cambridge, Department of Chemistry, Cambridge, CB2 1EW, U.K.

Author Contributions

[⊗]Y.K., U.G., and O.E. contributed equally.

Notes

The authors declare no competing financial interest.

■ ACKNOWLEDGMENTS

The research leading to these results has received funding from the Deutsche Forschungsgemeinschaft [grant number BA 4046/1-2] to S.B., the Swedish Research Council and the Knut and Alice Wallenberg Foundation to G.W. and the International Max Planck Research School on Multiscale Biosystems to S.K. We thank Nils Carlin (Scandinavian Biopharma) for providing us with *Shigella flexneri* oligo- and polysaccharide preparations. We thank Sebastian Mahlow for assistance with CE-LIF and Mandy Schietke for excellent technical assistance. We thank the staff at BESSY II (Helmholtz-Zentrum Berlin) for support with diffraction experiments and Manfred Weiss for helpful discussions on data processing.

■ REFERENCES

(1) Whitfield, C.; Trent, M. S. *Annu. Rev. Biochem.* **2014**, *83*, 99.
(2) Mazmanian, S. K.; Liu, C. H.; Tzianabos, A. O.; Kasper, D. L. *Cell* **2005**, *122*, 107.
(3) Steinberg, N.; Kolodkin-Gal, I. *J. Bacteriol.* **2015**, *197*, 2092.
(4) Zimmermann, S.; Lepenies, B. In *Carbohydrate-Based Vaccines: Methods and Protocols*; Lepenies, B., Ed.; Springer: Clifton, NJ, 2015; Vol. *1331*.
(5) Kuttel, M. M.; Jackson, G. E.; Mafata, M.; Ravenscroft, N. *Carbohydr. Res.* **2015**, *406*, 27.
(6) Haji-Ghassemi, O.; Blackler, R. J.; Martin Young, N.; Evans, S. V. *Glycobiology* **2015**, *25*, 920.
(7) Little, D. J.; Li, G.; Ing, C.; DiFrancescoc, B. R.; Bamford, N. C.; Robinson, H.; Nitz, M.; Pomes, R.; Howell, P. L. *Proc. Natl. Acad. Sci. U. S. A.* **2014**, *111*, 11013.
(8) Vulliez-Le Normand, B.; Saul, F. A.; Phalipon, A.; Belot, F.; Guerreiro, C.; Mulard, L. A.; Bentley, G. A. *Proc. Natl. Acad. Sci. U. S. A.* **2008**, *105*, 9976.
(9) Battistel, M. D.; Shangold, M.; Trinh, L.; Shiloach, J.; Freedberg, D. I. *J. Am. Chem. Soc.* **2012**, *134*, 10717.
(10) Woods, R. J.; Tessier, M. B. *Curr. Opin. Struct. Biol.* **2010**, *20*, 575.
(11) Widmalm, G. A. *Carbohydr. Res.* **2013**, *378*, 123.
(12) Andres, D.; Baxa, U.; Hanke, C.; Seckler, R.; Barbirz, S. *Biochem. Soc. Trans.* **2010**, *038*, 1386.
(13) Steinbacher, S.; Baxa, U.; Miller, S.; Weintraub, A.; Seckler, R.; Huber, R. *Proc. Natl. Acad. Sci. U. S. A.* **1996**, *93*, 10584.
(14) Schulz, E. C.; Schwarzer, D.; Frank, M.; Stummeyer, K.; Muhlenhoff, M.; Dickmanns, A.; Gerardy-Schahn, R.; Ficner, R. *J. Mol. Biol.* **2010**, *397*, 341.
(15) Barbirz, S.; Muller, J. J.; Uetrecht, C.; Clark, A. J.; Heinemann, U.; Seckler, R. *Mol. Microbiol.* **2008**, *69*, 303.
(16) Barry, E. M.; Pasetti, M. F.; Sztein, M. B.; Fasano, A.; Kotloff, K. L.; Levine, M. M. *Nat. Rev. Gastroenterol. Hepatol.* **2013**, *10*, 245.
(17) Jonsson, K. H. M.; Säwén, E.; Widmalm, G. *Org. Biomol. Chem.* **2012**, *10*, 2453.
(18) Kang, Y.; Barbirz, S.; Lipowski, R.; Santer, M. *J. Phys. Chem. B* **2014**, *118*, 2523.
(19) West, N. P.; Sansonetti, P.; Mounier, J.; Exley, R. M.; Parsot, C.; Guadagnini, S.; Prévost, M. C.; Prochnicka-Chalufour, A.; Delepierre, M.; Tanguy, M.; Tang, C. M. *Science* **2005**, *307*, 1313.
(20) Simmons, D. A. R.; Romanowska, E. *J. Med. Microbiol.* **1987**, *23*, 289.
(21) Lindberg, A. A.; Wollin, R.; Gemski, P.; Wohlhieter, J. A. *J. Virol.* **1978**, *27*, 38.
(22) Freiberg, A.; Morona, R.; Van den Bosch, L.; Jung, C.; Behlke, J.; Carlin, N.; Seckler, R.; Baxa, U. *J. Biol. Chem.* **2003**, *278*, 1542.
(23) Muller, J. J.; Barbirz, S.; Heinle, K.; Freiberg, A.; Seckler, R.; Heinemann, U. *Structure* **2008**, *16*, 766.
(24) Dixon, A. M.; Venable, R.; Widmalm, G.; Bull, T. E.; Pastor, R. W. *Biopolymers* **2003**, *69*, 448.
(25) Jayalakshmi, V.; Krishna, N. R. *J. Magn. Reson.* **2002**, *155*, 106.
(26) Baxa, U.; Cooper, A.; Weintraub, A.; Pfeil, W.; Seckler, R. *Biochemistry* **2001**, *40*, 5144.
(27) McNamara, J. T.; Morgan, J. L. W.; Zimmer, J. A. *Annu. Rev. Biochem.* **2015**, *84*, 895.
(28) Woodward, R.; Yi, W.; Li, L.; Zhao, G.; Eguchi, H.; Sridhar, P. R.; Guo, H.; Song, J. K.; Motari, E.; Cai, L.; Kelleher, P.; Liu, X.; Han, W.; Zhang, W.; Ding, Y.; Li, M.; Wang, P. G. *Nat. Chem. Biol.* **2010**, *6*, 418.
(29) Ruiz, N.; Kahne, D.; Silhavy, T. J. *Nat. Rev. Microbiol.* **2009**, *7*, 677.
(30) Kadirvelraj, R.; Gonzalez-Outeirino, J.; Foley, B. L.; Beckham, M. L.; Jennings, H. J.; Foote, S.; Ford, M. G.; Woods, R. J. *Proc. Natl. Acad. Sci. U. S. A.* **2006**, *103*, 8149.
(31) Parent, K. N.; Erb, M. L.; Cardone, G.; Nguyen, K.; Gilcrease, E. B.; Porcek, N. B.; Pogliano, J.; Baker, T. S.; Casjens, S. R. *Mol. Microbiol.* **2014**, *92*, 47.
(32) Theillet, F. X.; Frank, M.; Vulliez-Le Normand, B.; Simenel, C.; Hoos, S.; Chaffotte, A.; Bélot, F.; Guerreiro, C.; Nato, F.; Phalipon, A.; Mulard, K. A.; Delepierre, M. *Glycobiology* **2011**, *21*, 1570.
(33) Kirschner, K. N.; Yongye, A. B.; Tschampel, S. M.; Gonzalez-Outeirino, J.; Daniels, C. R.; Foley, B. L.; Woods, R. J. *J. Comput. Chem.* **2008**, *29*, 622.
(34) Guvench, O.; Hatcher, E.; Venable, R. M.; Pastor, R. W.; MacKerell, A. D., Jr. *J. Chem. Theory Comput.* **2009**, *5*, 2353.
(35) Bras, N. F.; Cerqueira, N. M. F. S. A.; Fernandes, P. A.; Ramos, M. J. *Int. J. Quantum Chem.* **2008**, *108*, 2030.
(36) Darveau, R. P.; Hancock, R. E. *J. Bacteriol.* **1983**, *155*, 831.

DOI: 10.1021/jacs.6b00240
J. Am. Chem. Soc. 2016, 138, 9109−9118

(37) Mueller, U.; Darowski, N.; Fuchs, M. R.; Foerster, R.; Hellmig, M.; Paithankar, K. S.; Puehringer, S.; Steffien, M.; Zocher, G.; Weiss, M. S. *J. Synchrotron Radiat.* **2012**, *19*, 442.
(38) Krug, M.; Weiss, M.; Heinemann, U.; Mueller, U. *J. Appl. Crystallogr.* **2012**, *45*, 568.
(39) Evans, P. *Acta Crystallogr., Sect. D: Biol. Crystallogr.* **2006**, *62*, 72.
(40) McCoy, A. J.; Grosse-Kunstleve, R. W.; Adams, P. D.; Winn, M. D.; Storoni, L. C.; Read, R. J. *J. Appl. Crystallogr.* **2007**, *40*, 658.
(41) Bailey, S. *Acta Crystallogr., Sect. D: Biol. Crystallogr.* **1994**, *50*, 760.
(42) Langer, G.; Cohen, S.; Lamzin, V.; Perrakis, A. *Nat. Protoc.* **2008**, *3*, 1171.
(43) Emsley, P.; Cowtan, K. *Acta Crystallogr., Sect. D: Biol. Crystallogr.* **2004**, *60*, 2126.
(44) Murshudov, G. N.; Vagin, A. A.; Dodson, E. J. *Acta Crystallogr., Sect. D: Biol. Crystallogr.* **1997**, *53*, 240.
(45) Bricogne, G.; Blanc, E.; Brandl, M.; Flensburg, C.; Keller, P.; Paciorek, W.; Roversi, P.; Sharff, A.; Smart, O. S.; Vonrhein, C.; Womack, T. O. *BUSTER*; Global Phasing Ltd.: Cambridge, United Kingdom, 2011.
(46) *PyMOL*; SchroedingerLLC, 2015.
(47) Wagner, R.; Berger, S. *J. Magn. Reson., Ser. A* **1996**, *123*, 119.
(48) Thrippleton, M. J.; Keeler, J. *Angew. Chem., Int. Ed.* **2003**, *42*, 3938.
(49) Landström, J.; Nordmark, E. L.; Eklund, R.; Weintraub, A.; Seckler, R.; Widmalm, G. *Glycoconjugate J.* **2008**, *25*, 137.
(50) Mayer, M.; Meyer, B. *Angew. Chem., Int. Ed.* **1999**, *38*, 1784.
(51) Mayer, M.; Meyer, B. *J. Am. Chem. Soc.* **2001**, *123*, 6108.
(52) Krishna, N.; Jayalakshmi, V. *Prog. Nucl. Magn. Reson. Spectrosc.* **2006**, *49*, 1.
(53) Rundlöf, T.; Venable, R. M.; Pastor, R. W.; Kowalewski, J.; Widmalm, G. *J. Am. Chem. Soc.* **1999**, *121*, 11847.
(54) Jayalakshmi, V.; Krishna, N. R. *J. Am. Chem. Soc.* **2005**, *127*, 14080.
(55) Han, B.; Liu, Y.; Ginzinger, S. W.; Wishart, D. S. *J. Biomol. NMR* **2011**, *50*, 43.
(56) Ulrich, E. L.; Akutsu, H.; Doreleijers, J. F.; Harano, Y.; Ioannidis, Y. E.; Lin, J.; Livny, M.; Mading, S.; Maziuk, D.; Miller, Z.; Nakatani, E.; Schulte, C. F.; Tolmie, D. E.; Wenger, R. K.; Yao, H.; Markley, J. L. *Nucleic Acids Res.* **2008**, *36*, D402.
(57) Andres, D.; Roske, Y.; Doering, C.; Heinemann, U.; Seckler, R.; Barbirz, S. *Mol. Microbiol.* **2012**, *83*, 1244.
(58) Malinova, I.; Mahlow, S.; Alseekh, S.; Orawetz, T.; Fernie, A. R.; Baumann, O.; Steup, M.; Fettke, J. *Plant Physiol.* **2014**, *164*, 907.
(59) Duan, Y.; Wu, C.; Chowdhury, S.; Lee, M. C.; Xiong, G. M.; Zhang, W.; Yang, R.; Cieplak, P.; Luo, R.; Lee, T.; Caldwell, J.; Wang, J. M.; Kollman, P. *J. Comput. Chem.* **2003**, *24*, 1999.
(60) Klauda, J. B.; Venable, R. M.; Freites, J. A.; O'Connor, J. W.; Tobias, D. J.; Mondragon-Ramirez, C.; Vorobyov, I.; MacKerell, A. D., Jr.; Pastor, R. W. *J. Phys. Chem. B* **2010**, *114*, 7830.
(61) Van der Spoel, D.; Lindahl, E.; Hess, B.; Groenhof, G.; Mark, A. E.; Berendsen, H. J. C. *J. Comput. Chem.* **2005**, *26*, 1701.
(62) Case, D. A.; Darden, T. A.; Cheatham, III, T. E.; Simmerling, C. L.; Wang, J.; Duke, R. E.; Luo, R.; Walker, R. C.; Zhang, W.; Merz, K. M.; Roberts, B.; Wang, B.; Hayik, S.; Roitberg, A.; Seabra, G.; Kolossváry, I.; Wong, K. F.; Paesani, F.; Vanicek, J.; Liu, J.; Wu, X.; Brozell, S. R.; Steinbrecher, T.; Gohlke, H.; Cai, Q.; Ye, X.; Wang, J.; Hsieh, M. J.; Cui, G.; Roe, D. R.; Mathews, D. H.; Seetin, M.G.; Sagui, C.; Babin, V.; Luchko, T.; Gusarov, S.; Kovalenko, A.; Kollman, P. A. *Amber11*; University of California: San Francisco, 2010.
(63) Wehle, M.; Vilotijevic, I.; Lipowsky, R.; Seeberger, P. H.; Silva, D. V.; Santer, M. *J. Am. Chem. Soc.* **2012**, *134*, 18964.
(64) Martyna, G. J.; Klein, M. L.; Tuckerman, M. *J. Chem. Phys.* **1992**, *97*, 2635.
(65) Darden, T.; York, D.; Pedersen, L. *J. Chem. Phys.* **1993**, *98*, 10089.
(66) Miyamoto, S.; Kollman, P. A. *J. Comput. Chem.* **1992**, *13*, 952.
(67) Hess, B.; Bekker, H.; Berendsen, H. J. C.; Fraaije, J. *J. Comput. Chem.* **1997**, *18*, 1463.
(68) Morris, G. M.; Huey, R.; Lindstrom, W.; Sanner, M. F.; Belew, R. K.; Goodsell, D. S.; Olson, A. J. *J. Comput. Chem.* **2009**, *30*, 2785.
(69) Kumar, S.; Bouzida, D.; Swendsen, R. H.; Kollman, P. A.; Rosenberg, J. M. *J. Comput. Chem.* **1992**, *13*, 1011.

DOI: 10.1021/jacs.6b00240
J. Am. Chem. Soc. 2016, 138, 9109−9118